Fermi National Accelerator Laboratory
PO Box 500
Batavia, IL 60510
TD-05-020
April 2005

A Comparison of Q-Slope Models and Data in Bulk Nb SRF Cavities

P. Bauer[1,1], G.L. Ciovati[2], A. Gurevich[3], L. Lilje[4], N. Solyak[1], B. Visentin[5]

(1) Fermilab, (2) Jefferson Lab, (3) ASC-University of Wisconsin, (4) DESY, (5) CEA-Saclay

April 20th 2005

1) Introduction

Very powerful RF cavities are now being developed for future large-scale particle accelerators using niobium superconductor. Today's prototype cavities operate in RF surface magnetic fields of up to *180 mT*. This is the result of a successful worldwide technology development effort over the last decades.

The basic model for Q-slope in SRF cavities, i.e. the reduction of the cavity quality factor with increasing operating electric and magnetic fields, is the so-called thermal feedback model. The exponential dependence of the BCS surface resistance on temperature, in feedback with the dependence of the RF power dissipation on the surface resistance ultimately leads to thermal runaway (thermal quench) of the RF exposed surface. Before investigating further the high field surface resistance it is important to understand better the basic Q slope (or surface resistance increase with applied RF field amplitude) due to thermal feedback.

The main purpose of this note is to compare calculations of Q-slope on the basis of the BCS resistance and the thermal feedback model with experimental data from cavities. The discussion encompasses a wide variety of cavities from DESY, CEA-Saclay, J-Lab and Fermilab. This comparison also includes the non-linear correction to the BCS resistance as recently proposed by A. Gurevich.

[1] pbauer@fnal.gov

2) The Thermal Feedback Model

Although very small, some non-negligible heating occurs when superconducting RF cavities are operated at low temperature. The heat generated in the small (nΩ) surface resistance is conducted through the niobium bulk and evacuated by the liquid helium. In TM01 mode cavities most of the heat is generated in a several cm wide strip around the equator area of the cavity, where the magnetic field (and thus the surface current) is highest. The peak field area is large enough to allow for a one-dimensional representation of the thermal problem (see Fig. 0). The temperature profile across the niobium bulk and

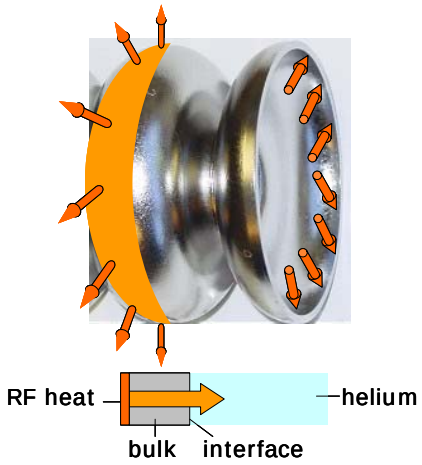

Figure 0: Schematic of thermal model on an a FNAL 3rd harmonic cavity prototype.

the temperature drop across the niobium-helium interface can be calculated exactly from the steady state heat balance equation (Eq. 1) and the temperature dependent thermal properties, conductivity κ and Kapitza conductance h_{Kap}. The thermal diffusivity (c_p/κ) of high purity niobium at low temperature is of the order of *0.01* m^2/sec, which, given *mm* thick walls result in a *msec* thermal equilibrium time. RF pulses are typically of that length (or longer) and therefore the process is reasonably well described as in steady state.

The following briefly summarizes the thermal feedback model. A more detailed discussion can be found in [1]. The steady state heat balance equation (Eq.1) consists of conduction and generation terms. The delta-function in the generation term reflects the fact that the RF heating is concentrated in a very thin layer. The RF power dissipated per unit area in the cavity depends on the RF magnetic field amplitude H_{RF} and the (temperature dependent) RF surface resistance $R_s(T)$ as given in Eq. 2. The equation assumes that the loss is due to the RF shielding currents only and neglects the contribution by electric surface fields.

$$\frac{\partial}{\partial x}\kappa(T)\frac{\partial T}{\partial x} + P_{diss}(T_m, H_c, ..)\delta(x) = 0 \qquad \left(\frac{W}{m^2}\right) \tag{1}$$

$$P_{diss} = \frac{1}{2} R_s(T_m) H_{RF}^2 \qquad \left(\frac{W}{m^2}\right) \tag{2}$$

The solution of Eq. 1 depends on the surface temperatures on both sides of the niobium sheet. The temperature on the RF exposed side, T_m, drives the surface resistance, while the temperature on the helium side, T_s, determines the Kapitza conductance. They can be derived exactly from the boundary conditions (Eqs. 3 & 4).

$$h_{Kap}(T_s, T_0)\,d(T_s - T_0) = \int_{T_s}^{T_m} \kappa(T')\,dT' \qquad \left(\frac{W}{m}\right) \tag{3}$$

$$\frac{1}{2} R_s(T_m, H_c, ..) H_{RF}^2 = h_{Kap}(T_s, T_0)(T_s - T_0) \qquad \left(\frac{W}{m^2}\right) \tag{4}$$

Eqs. (3) & (4) can be solved for T_m and T_s, for a given H_{RF}, T_0 and R_s $(T_m, H_{RF}, ..)$. In the remainder of this discussion we will use the exact, numerical solutions of Eqs. (3)&(4). Appendix 2, however, also discusses the issues related to an analytical model, which is often (and should not be) used in other, similar publications.

The strong temperature dependence of the BCS resistance is at the core of the thermal feedback. According to this model the increase of the surface resistance with field is the result of a feedback process during which the surface temperature increases due to RF heating while the RF heating increases with surface temperature. The feedback is strong because of the exponential dependence of the BCS surface resistance on temperature. In this process the cavity surface temperature ultimately runs away and the thermal model therefore could, in the absence of other limitations (such as the critical magnetic field), also predict the magnetic field at which the cavity quenches. The quench field due to thermal feedback is typically referred to as "thermal quench field" (as opposed to the critical field).

3) RF Surface Resistance

The RF surface resistance is still subject of intense research. Some surface resistance contributions are better known than others. Eq. 5 lists the contributions that are more or less known. They are the BCS resistance ($R_{s,BCS}$), the residual resistance (R_{res}), the surface resistance due to field enhancement on grain edges ($R_{s,FE}$), the surface resistance due to trapped magnetic flux ($R_{s,Btrap}$). The main parameters on which they depend are also listed.

$$R_{s,RF} = R_{s,BCS}(T_m, H_{DC}, H_{RF}) + R_{res}(\omega, T, ..) + R_{s,FE}(H_{RF}, \beta) + R_{s,Btrap}(H_0) + ... \qquad (\Omega) \tag{5}$$

The BCS RF surface resistance is the result of the interaction between the RF fields (penetrating λ deep into the surface) and the thermally activated electrons above the energy gap in the superconductor. A widely used, simplified version of the linear BCS resistance is as given in Eq. (6), where the gap parameter α is the superconducting energy gap, Δ, normalized on $k_B T_c$. The more fundamental equation, which, in the clean limit, depends on the gap energy ($\Delta \sim 3\ meV$) and ξ and λ the coherence length and penetration depth (both $\sim 40\ nm$), is discussed in [1]. The material parameters Δ, ξ, λ vary strongly throughout the penetration depth of the superconductor due to the presence of metallic oxides and defects on the surface and along grain boundaries. Therefore, in the absence of exact parameter profiles of the material in the cavities, the linear BCS surface resistance is typically written in the simpler form as in Eq. 6 with the understanding that the parameters $A(\omega)$ and α are actually averages of the fundamental parameters (Δ, ξ, λ) over λ.

$$R_{s,BCS}(T) = A(\omega)\frac{T_c}{T}e^{-\alpha\frac{T_c}{T}} \quad (\Omega) \tag{6}$$

As discussed in further detail in [1], Eq. 6 gives the linear BCS surface resistance, i.e. the BCS contribution at fields much lower than the critical field. At fields approaching the critical field, distortions of the electronic band structure in the superconductor occur, leading to additional quasi-particle excitation above the gap and increased BCS loss. The first critical field correction term to BCS according to [1] is:

$$R_{s,BCS}(T, H_{RF}) = R_{s,BCS}(T, H_{RF} = 0)\left[1 + C(T,\omega)\left(\frac{H_{RF}}{H_c}\right)^2 + \ldots\right] \quad (\Omega) \tag{7}$$

where C is a constant that can be calculated from material parameters and is of order unity in Nb at ~ 2 K. C as introduced in [1] is approximately given in Eq. 8 (this approximation is not valid for T→0, for instance). C increases above one at lower temperature and with higher frequency. The larger C becomes the less valid the first order development in Eq. 7 becomes. The term $\mu_0 H_c$ is the thermodynamic critical field (~180 mT). The highest field reached in cavities to-date is very close to it[2], suggesting that it could also be the RF critical field (the most optimistic projections invoke the so-called superheating field which is ~20% above H_c in Nb).

$$C(T,\omega) = \frac{\pi^2}{384}\left[1 + \frac{\ln(9)}{3\ln\left(4.1\frac{k_B T\Delta}{(\hbar\omega)^2}\left(\frac{\xi}{\lambda}\right)^2\right)}\right]\left(\frac{\Delta}{k_B T}\right)^2 \tag{8}$$

The BCS resistance, which is strongly temperature dependent, can be derived from Q measurements in the cavity at different temperatures. The fit of the temperature

dependence of the surface resistance allows to separate temperature dependent (BCS) and independent (residual,..) surface resistance contributions. This procedure is easiest (and usually applied) at low field. At high fields the low and high field BCS contributions need to be disentangled, adding difficulty to the procedure.

4) General Discussion of the Thermal Feedback Model

As discussed in further detail in [1], some general trends of the thermal feedback model can be derived. The general characteristics are a useful guide to a better understanding of the "thermal" Q-slope. For instance, a simplified implementation of the thermal feedback model can be used to calculate the thermal breakdown field. For that purpose the basic equations of the model are simplified (as discussed further in Appendix 2) to provide an expression for $H_{RF}(T)$:

$$H_{RF}^2 = \frac{2(T_m - T_0)}{R_s(T_m)}\left(\frac{\kappa h_{Kap}}{d h_{Kap} + \kappa}\right) \quad \left(\frac{A^2}{m^2}\right) \tag{9}$$

After inserting the linear BCS resistance (neglecting all other surface resistance contributions including the residual resistance) as stated in Eq. 6 one obtains:

$$H_{RF}^2 = \frac{2(T_m - T_0)T_m}{A(\omega)T_c} e^{\frac{\alpha T_c}{T_m}}\left(\frac{\kappa h_{Kap}}{d h_{Kap} + \kappa}\right) \quad \left(\frac{A^2}{m^2}\right) \tag{10}$$

As discussed in [1] the above expression goes through a maximum with the exponential rise of the surface resistance reducing the equilibrium surface heat dissipation at surface temperatures beyond the maximum. The region of surface temperature at which H_{RF}^2 is below the maximum is that where the surface heating is less than could be transported to the helium in the steady state. The maximum RF field and the maximum allowable surface temperature can be found from Eq. 10. The surface temperature at which the RF field peaks is typically *~0.3 K* above bath temperature in TESLA type bulk Nb cavities.

The peak surface temperature can also be calculated from the derivative of Eq. 10 $d(H_{RF}^2)/dT=0$. As shown in [1] the approximate solution for the peak temperature is $T_{max} \sim T_0 + T_0^2/(\alpha T_c)$. This result shows that the maximum overheating is, in first approximation, independent of the material properties and only a function of the gap parameter and the bath temperature. For the bath temperature of *1.8 K*, T_{max} becomes *1.97 K*, *0.17 K* above T_0. This illustrates how little overheating is actually needed to thermally quench the cavity. This fact explains why the heat balance equation (Eq. 1) of the thermal feedback model can often be simplified for approximate solutions using constant thermal properties. The maximum temperature can also be used to estimate the Q-drop at the thermal quench field from the ratio of the surface resistances at T_0 and T_{max}. If one neglects the residual resistance and takes into account only the linear term of the BCS resistance the ratio becomes *e*.

Appendix 2 compares an analytical with the numerical (exact) implementation of the thermal feedback model. More can be learned about the thermal feedback there.

5) Comparison of Thermal Feedback Model with Cavity Data

The following presents a comparison of model and experimental data. The model implementation used in this comparison is a numerical model that solves exactly Eq.3&4. The thermal feedback model used the residual and the linear BCS surface resistances measured in the cavities at low field (the BCS fit parameters α and Δ as well as $R_{s,res}$ are listed together with the data in Table 1). Model calculations were performed with and without the non-linear correction (Eq. 7&8) to the BCS resistance. The material properties (thermal conductivity and Kapitza conductance) were calculated with the functional implementations discussed in appendix 1 ((A1-6) & (A1-7)). The thermal parameters calculated at the bath temperature are listed together with the calculation results as well as in Table 1. Note that the different cavities were often tested at different bath temperatures. Also note that the model implementation here assumes uniform surface properties and does therefore not include the "hot" or "weak" spots that most likely exists in a real cavity.

The most important criterion the experimental data needed to satisfy for this comparison is that they needed to have as little Q slope as possible, such as to reduce as much as possible the surface resistance to the basic residual and BCS components. This condition should obviously improve the agreement between data and model, with the model using only BCS (and residual) resistance. All the cavity experimental results discussed here were chosen with this criterion in mind. Most cavities were reduced size prototypes, with the only exception being the DESY AC70, which is a full-length 9-cell TESLA cavity. The Saclay and DESY cavities were electro-polished, while the J-Lab and FNAL cavities were BCP etched. The J-Lab cavities and the Saclay cavity C115 were also post-purified (heat treated at ~1400°C in the presence of Ti to increase RRR). The thermal conductivity function was not modified to account for the increased RRR. The data obtained before and after the low temperature (~120°C, 50 hrs) bake are presented. Essentially all Q measurements were performed in the CW (=steady state) mode.

Table 1 summarizes the experimental and model parameters used in the comparison. The thermal parameters given in the table were calculated at the bath temperature (see appendix 1 for the material parameter functions). The parameters for the linear BCS and residual resistance were derived from fits of measurements of the surface resistance as function of temperature at low power. In this procedure the residual resistance is the value to which the $R_s(T)$ data tend at very low temperature, where the BCS resistance vanishes. The parameter for the nonlinear contribution $C(T.\omega)$ was calculated with Eq. 8 with the respective Δ obtained from the fits of the low power linear BCS resistance data. The material parameters ξ and λ were assumed to be 40 nm.

Table 1: Summary table for data vs model comparison. Parameters for the model calculations: Linear (Δ/k_BT_c, $A(\omega)$, Eq. 6) and non-linear BCS resistance ($C(T_0,\omega)$, Eq. 7&8), thermal conductivity (κ, Eq. A1-6) and Kapitza conductance (h_{Kap}, Eq. A1-7). Data out(inside) parentheses are for before(after) the low temperature bake. * assumed values.

	C-103	C-115	D-AC70	F-3C-1	J-LLSC	J-OCSC
T_0 (K)	1.44	1.6	2 (1.9)	1.8	2.0	1.4
G (Ω)	283	283	270	291	282	273
d (mm)	2.6	2.6	2.6	2.6	2.6	2.6
$\kappa(T_0)$ (W/K/m)	6.1	7.6	11.22	9.9	12.7	5.8
$h_{Kap}(T_0)$ (W/K/m^2)	1090	1780	3956	3080	5021	956
RRR *	300	300	300	300	300	300
R_{res} (nΩ)	3.2 (4.2)	1 (2)	-10 (5.2)	10	17 (9.4)	3.6 (5)
$R_{bcs,lin}(T_0)$ (nΩ)	0.5 (0.3)	1.7 (1.05)	24 (4.3)	40	31 (20)	3.9 (5.1)
Δ/k_BT_c	2 (2.05)	1.97 (1.93)	1.53 (1.94)	1.92	2.1 (1.94)	2.09 (2.15)
$A(\omega)$ (10^{-5} Ω)	2.76(2.13)	2.5 (1.2)	0.597(1.058)	14.8	4.4 (1.7)	4.46 (2.38)
T_c (K) *	9.2	9.2	9.2	9.2	9.2	9.2
$\omega/2\pi$ (GHz)	1.3	1.3	1.3	3.9	1.5	1.5
$C(T_0,\omega)$	4.5 (4.5)	3.6 (3.4)	1.5 (2.5)	2.9	2.6 (2.2)	5.2 (5.5)
μ_0H_c (mT) *	180	180	180	180	180	180

Figure 1 compares the model results with the state of the art electro-polished TESLA single cell cavity C-103, manufactured and tested at CEA/Saclay [3]. After baking this cavity is among the best ever tested, reaching surface fields consistent with a 40 MV/m average accelerating gradient. As becomes clear in this comparison the thermal feedback model under-estimates the Q slope in the cavities, even after baking. This discrepancy remains even after taking into account the non-linear BCS component (Eqs. (7)&(8)). Furthermore, even strongly reduced thermal properties do not result in a better agreement. Could this be an indication for an additional surface resistance contribution?

Also of interest is that the steep slope at ultimate fields in the non-baked case appears to clearly depart from the Q characteristic that the thermal feedback models predict. The slope is almost exponential and cannot be fitted with any n as in H_{RF}^n. Figure 2 shows a similar situation as in Figure 1, except that it is for a different cavity (CEA/Saclay–C-115). Differently from C-103, the data can be fitted with the model including the non-linear BCS contribution (while it cannot when using only the linear BCS resistance). As before in the case of C-103 the ultimate Q-slope before baking cannot be fitted with any BCS resistance implementation.

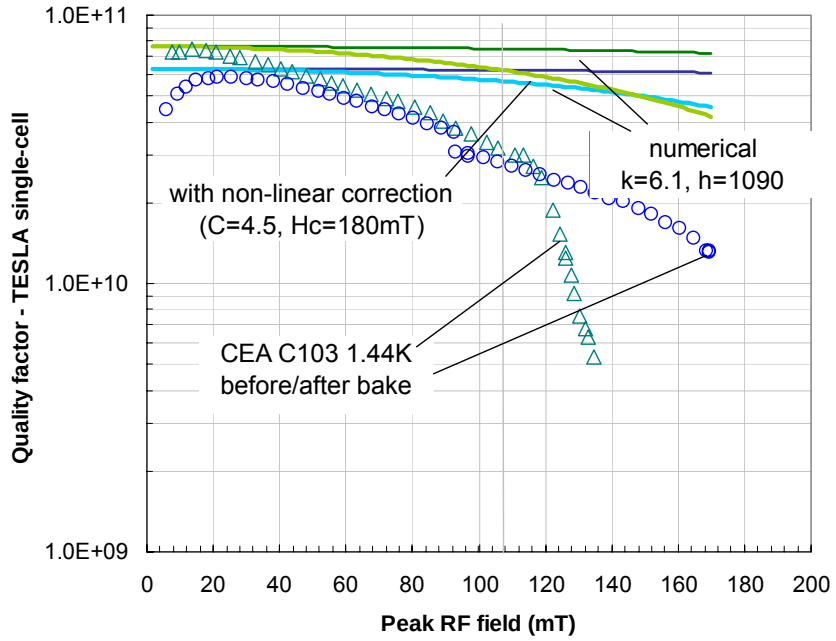

Figure 1: Comparison of measured and predicted quality factor of a CEA/Saclay single cell TESLA cavity (C 103) before and after baking. Experimental data were obtained at 1.44 K.

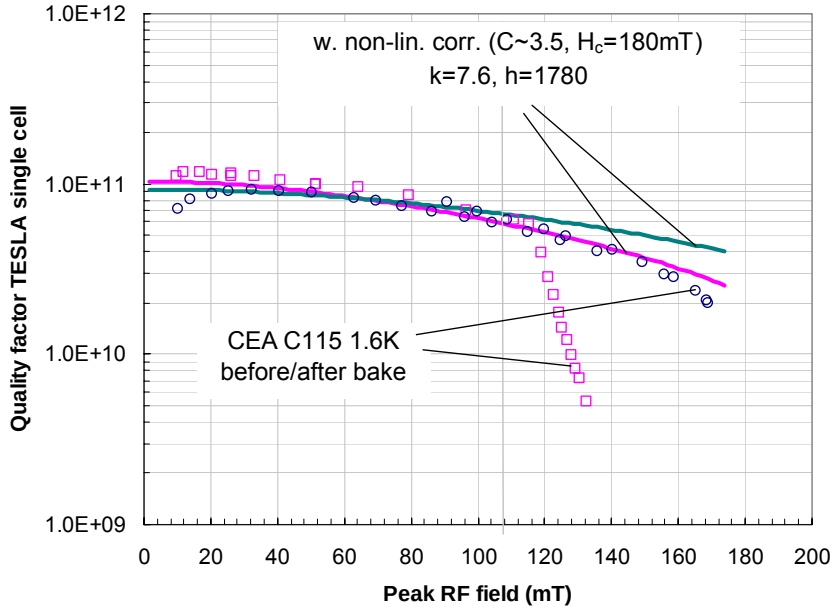

Figure 2: Comparison of measured and predicted quality factor of a CEA/Saclay single cell TESLA cavity (C 115) before and after baking. Experimental data were obtained at 1.6 K.

Among the best DESY cavities is AC70, a 9-cell TESLA cavity. The comparison between experimental data and those obtained with the thermal feedback model is shown in Figure 3. The comparison shows that the thermal feedback model with linear BCS resistance only, underestimates the data before and after baking for most fields. The

inclusion of the non-linear contribution yields a better agreement between data and model. The non-linear model in fact overestimates the Q-slope in the mid-to-high field region. An increased thermal conductivity could in part reduce the discrepancy. This would produce a case that is very similar to the Saclay C 115 case discussed above. Again, as with C-103 and C-115, the ultimate Q slope of AC70 before quenching of before (but also after) baking is not well described by the thermal feedback model.

The results obtained on a high-performance, low-loss J-Lab CEBAF type (1.5 GHz) single-cell cavity (LLSC) can be described in similar terms as those of DESY AC70 and Saclay C-115. The inclusion of the non-linear BCS resistance describes the medium field Q-slope reasonably well, while the linear BCS resistance alone underestimates the Q-slope (Figure 4). A (four-fold) increase of the thermal conductivity would produce exact agreement in that field region. Similarly as in the cases discussed above, the ultimate Q-slope before baking, however, is steeper than the prediction on the basis of even the non-linear model and any more or less realistic set of thermal parameters.

Interestingly, a different CEBAF single cell cavity, OCSC (original CEBAF shape), recently built at J-Lab, shows a behavior reminiscent of the Saclay cavity shown in Figure 1, where the medium field Q-slope is stronger than described by the thermal feedback model even with the non-linear BCS resistance. This cannot be "repaired", even with an extremely low thermal conductivity. That is at odds with the LLSC example shown in Figure 4. It is noteworthy that both the Saclay C-103 and the J-Lab OCSC cavities were tested at very low temperature (~1.4 K). Could that indicate that the prediction of the non-linear resistance with Eq. 8 underestimates the increase of the non-linear component at lower temperature? Or is there an additional, yet unknown surface resistance contribution that appears at temperatures below 1.5 K?

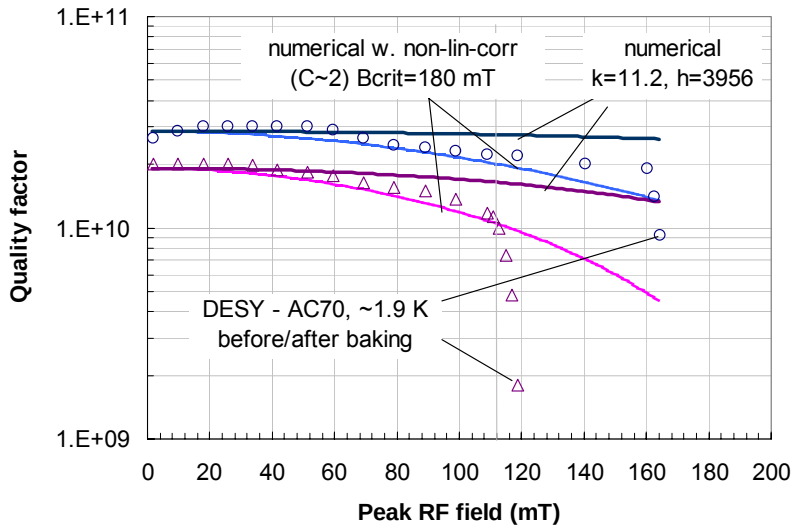

Figure 3: Comparison of measured and predicted quality factor of a DESY 9-cell TESLA cavity (AC70) before and after baking. Experimental data were obtained at ~1.9 K.

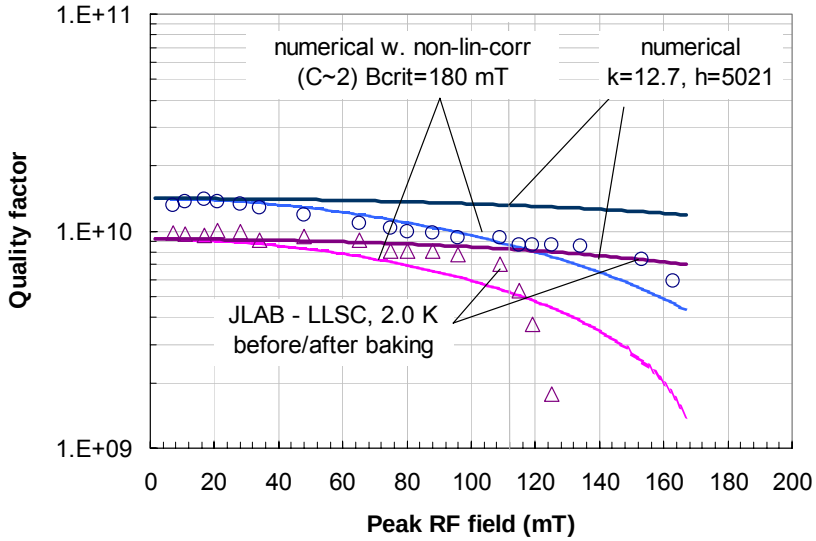

Figure 4: Comparison of measured and predicted quality factor of a JLAB low loss, single cell CEBAF cavity (LLSC, 1.5 GHz) before and after baking. Experimental data were obtained at 2.0 K.

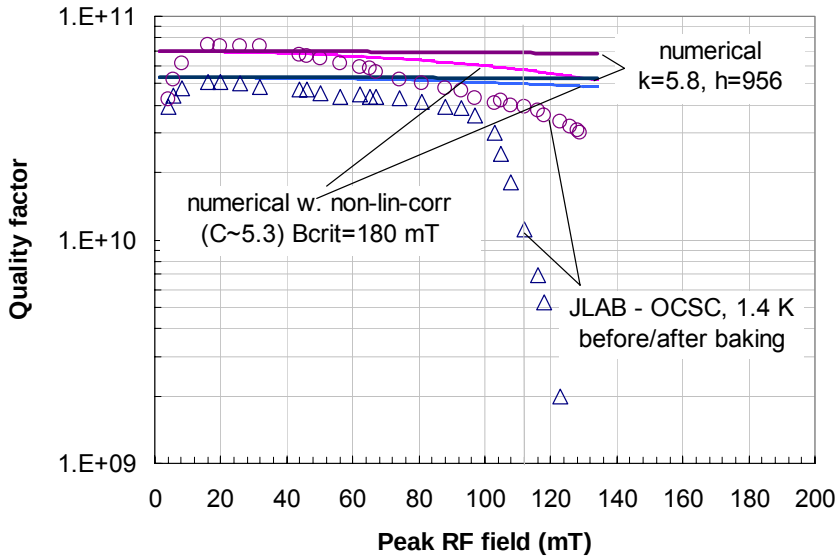

Figure 5: Comparison of measured and predicted quality factor of a JLAB single cell CEBAF cavity (OCSC – original CEBAF shape, 1.5 GHz) before and after baking. Experimental data were obtained at 1.4 K.

The Fermilab 3.9 GHz cavities represent a special case because of their higher frequency and the therefore increased BCS resistance by one order of magnitude. Figure 6 shows the model/experiment comparison for the first 3-cell 3rd harmonic prototype. The Q-slope and quench field (~105 mT) are more or less consistent with that predicted with the thermal feedback model including only the linear BCS resistance. The model predicts a quench field of 115 mT in this case. This clearly shows that the FNAL 3rd harmonic

cavities, unlike the TESLA fundamental mode cavities, are actually limited by thermal quench. It is not clear why the non-linear BCS resistance as given in Eq. 8 does not appear to describe well the Q slope found in the experiment.

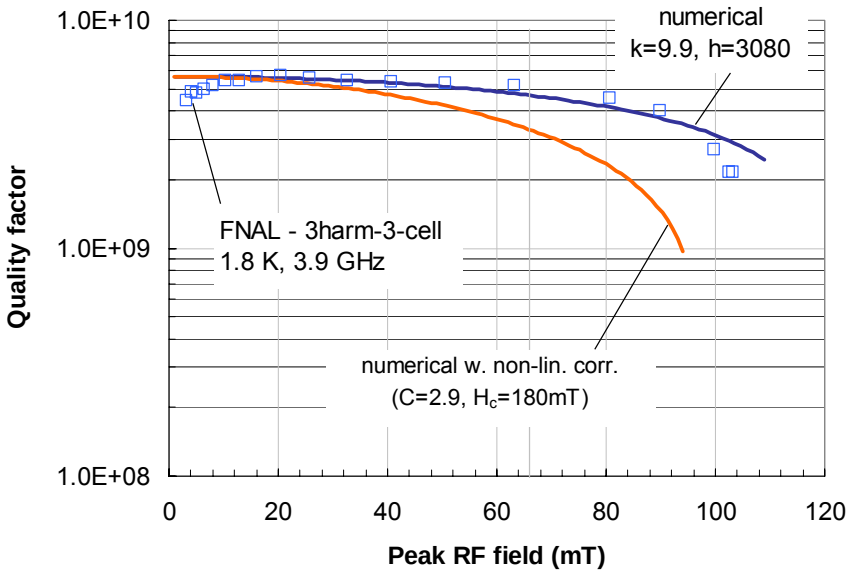

Figure 6: Comparison of measured quality factor of a Fermilab 3rd harmonic 3-cell cavity to model predictions. Experimental data were obtained at 1.8 K. The numerical model predicts the Q-slope as well as the quench field reasonably well.

6) Summary

Calculations based on the thermal feedback model were implemented and applied to the case of the state of the art SRF cavities from CEA, DESY, J-Lab and Fermilab. This comparison revealed the following features:

1) Thermal feedback models based only on linear BCS and residual surface resistance (as measured at low field in the respective cavities) under-estimate the Q-slope in the cases, in which the measurements were conducted at "typical" temperatures (~2 K). These cases require the inclusion of an additional surface resistance term, such as the non-linear BCS contribution suggested by Gurevich, [1].
2) Even the non-linear BCS surface resistance contribution is insufficient to describe the very steep, ultimate Q-slope found before baking.

The above observations, however, are contingent upon the assumptions made in the model, such as for instance the particular implementations of the thermal conductivity function or the choice of RF critical field. The RF critical field was not assumed to vary from the before to the after baking condition, for instance. A strong phonon-peak or other variations in the thermal conductivity or Kapitza conductance function can explain a certain level of disagreement between model and data. No realistic thermal parameters, however, can explain the ultimate Q-slope using the thermal feedback model used here.

Some "softer" conclusions can also be drawn from this comparison:

1) The Saclay C-103 and J-Lab-OCSC cavities, which were tested at lower temperatures than the others (discussed here) show a Q-slope that is more pronounced than that which can be described using the linear and non-linear BCS resistance contributions in the thermal feedback model. This observation was also made previously by several other groups (see for instance [3]). Reduced thermal parameters cannot explain this discrepancy. Could that indicate that the increase of non-linear BCS resistance is underestimated in Eq. 8?
2) The experimental data for the Fermilab 3rd harmonic cavity, which operates at 3.9 GHz, show that the data are well described with the model using linear BCS resistance and residual resistance only. Does this indicate that the non-linear BCS resistance model as formulated in Eq. 8 overestimates the non-linear BCS resistance increase at higher frequency?
3) The baking effect cannot be entirely be explained by the change of the linear BCS resistance as a result of a reduction of the *mfp* in the λ-layer. The above comparison shows that the ultimate Q-slope is not consistent with the linear BCS resistance and therefore this argument is invalid (in fact this was already previously pointed out by Visentin [4]).
4) Cavities with the low surface resistance levels as those discussed here (also assuming that they are defect free and not plagued by field emission) do not quench because of thermal runaway instability, but rather because they reach the RF critical field. The only exception to that case are the Fermilab 3.9 GHz cavities which operate at a higher BCS surface resistance and are therefore "thermally" limited (i.e. they quench because of thermal feedback).

A widely used and simple way to characterize Q-slope uses the so-called γ parameter from the R_s fit in Eq.11. A derivation of Eq.11 is given in Appendix 3.

$$R_s(H_{RF}) \approx R_s(T_0)\left[1+\gamma\left(\frac{H_{RF}}{H_{crit}}\right)^2\right] \tag{11}$$

Table 2 lists the γ parameters that fit the experimental data discussed in chapter 5. Note that the γ parameters in the first line represent the medium field Q-slope (for which the thermal feedback model is usually a good approximation). The parameters in the second line are those of the ultimate Q-slope, which cannot really be fitted by the thermal feedback model (as discussed above). The purpose of listing these numbers is to show that they are two orders of magnitude larger than those for the medium-field Q-slope. The predicted values on the basis of Eq. (A3-3) in Appendix 3 is $\gamma \sim 2$, close to the values listed in the first row of the table.

Table 2: Fit parameter γ (Eq. 25) for all experimental data discussed in chapter 6.

	C-103	C-115	D-A70	F-3C-1	LLSC	OCSC
γ (medium field)	3	3	1	1.5	1.5	2.6
γ (ultimate field)	500	350	500	-	500	650

Does this strong Q-slope before baking hint at a yet unknown surface resistance contribution? Could it be the result of a reduced critical RF field, below the 200 mT value assumed in this discussion? These are the questions that future research should resolve.

7) References

[1] A. Gurevich, "*Thermal RF breakdown of Superconducting Cavities", Proceedings of the "Pushing the Limits of RF Superconductivity*" workshop, Argonne National Lab, Sept 22-24 2004 http://www.aps.anl.gov/conferences/RFSC-Limits

[2] K. Saito, "*Fundamental RF Critical Field Overview*", Proceedings of the "Pushing the Limits of RF Superconductivity" workshop, Argonne National Lab, Sept 22-24 2004 http://www.aps.anl.gov/conferences/RFSC-Limits

[3] G. Ciovati, "*Effect of Low Temperature Baking on the Radio-Frequency Properties of Niobium Superconducting Cavities for Particle Accelerators*", Journal of Appl. Phys. Vol. 96/3, Aug. 2004, and
J. Halbritter, "*Electric Surface Resistance $R^{E}(T, f, E^{\perp})$ of Nb/Nb2O5-y-Interfaces and Q-Drop of Superconducting Nb Cavities*", IEEE Transactions on Applied Superconductivity, Vol. 11, No. 1, p. 1864, 2001

[4] B. Visentin "*Q-Slope at High Gradients: Review of Experiments and Theories*", RFSCWS 2003, Luebeck, Germany, Sept. 2003

Appendix 1) Thermal Material Parameters

A1-1) Thermal Conductivity

The following formalism for the thermal conductivity of high purity Niobium is from Koechlin-Bonin[2]. Their model uses modified material constants (indicated with ‘) and parameters to calibrate the theoretical model to measurement data. The total thermal conductivity is a sum of the electron and phonon contributions.

$$\boldsymbol{\kappa(T, RRR, A) = \kappa_{el}(T, RRR) + \kappa_{phon}(T, A)} \qquad \left(\frac{\boldsymbol{W}}{\boldsymbol{K-m}}\right) \tag{A1-1}$$

The electron contribution is regulated by the number of electrons at the Fermi-level, which are not condensed into the superconducting phase. A polynomial fit of the normalized superconducting electron function is (A1-2):

$$R(y) = 10^{-4}y^4 - 5.4\cdot 10^{-3}y^3 + 0.1017y^2 - 0.7848y + 2.1282 \qquad \alpha' < y < 8 \quad R(y>8) = 1 \tag{A1-2}$$

The electronic contributions to the thermal conductivity are given with Wiedemann-Franz ($L'=2.11x10^{-8} W\Omega/K^2$) and electron-phonon exchange ($F_{el\text{-}phon}=7.6x10^{-7} m/W/K$). Note that the argument of the superconducting electron function is $a'T_c/T$, with $a'=1.53$, the modified BCS gap parameter.

$$\kappa_{el}(T, RRR) = R\left(a'\frac{T_c}{T}\right)\frac{1}{\left(\frac{\rho(295K)}{L'\ RRR\ T}\right) + F_{el-phon}T^2} \qquad \left(\frac{W}{K-m}\right) \tag{A1-3}$$

The phonon contribution is given with $C_1=234\ mK^3/W$ and $C_2=4.34x10^3\ W/K^4/m^2$. Since the material considered is of very high purity, the phonon mean free path is assumed to be the grain-size.

$$\boldsymbol{\kappa_{phon}(T, A) = \frac{\left(1 + f_{peak}(A)\right)}{C_1 T^{-2} e^{-a'\frac{T_c}{T}} + \frac{1}{C_2 l_{mfp,phon} T^3}}} \qquad \left(\frac{\boldsymbol{W}}{\boldsymbol{K-m}}\right) \tag{A1-4}$$

The phonon-peak was (artificially) represented by a sin-function parameterized such as to generate a peak at 2 K with an (arbitrary) amplitude *A (~10-20)* (A1-5).

[2] F. Koechlin, B. Bonin, “Parametrisation of the Niobium Thermal Conductivity in the Superconducting State”, CEA internal note DAPNIA-SEA-96-01, Jan. 1996

$$f_{peak}(A) = A \cdot \sin\left((T - 0.5K)\frac{\pi}{2}\right) \qquad 1K < T < 3K \qquad \text{(A1-5)}$$

Figure 8 shows recent thermal conductivity data[3], indicating the presence of the phonon-peak in most instances. For a case including the phonon peak a simple fit can be used to approximately describe the thermal conductivity rather than using the full-blown Koechlin-Bonin model (Equ A1-6).

$$\kappa(T) = 0.7\ e^{(1.65T - 0.1T^2)} \qquad \left(\frac{W}{K - m}\right) \qquad \text{(A1-6)}$$

A1-2) Kapitza Conductance

A phenomenological fit for the Kapitza conductance for $T\text{-}T_0<1.4\ K$ was proposed by Mittag[4].

$$a_{Kap}(T) = 200 \cdot \left(T_0^{4.65}\right)\left[1 + 1.5\left(\frac{T - T_0}{T_0}\right) + \left(\frac{T - T_0}{T_0}\right)^2 + 0.25\left(\frac{T - T_0}{T_0}\right)^3\right] \quad \left(\frac{W}{Km^2}\right) \qquad \text{(A1-7)}$$

Figure 7 shows the Nb thermal conductivity calculated for RRR=300 with and without phonon-peak (*A=20*). Also shown is the calculation obtained with the fit (A1-6).

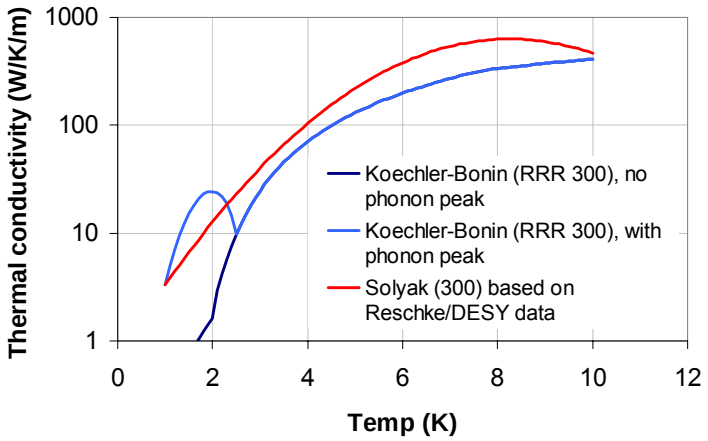

Figure 7: Thermal conductivity of high purity Nb (RRR=300) according to Koechlin-Bonin.

[3] Courtesy of D. Reschke / DESY
[4] Cryogenics, Vol. 13, p. 94, 1973

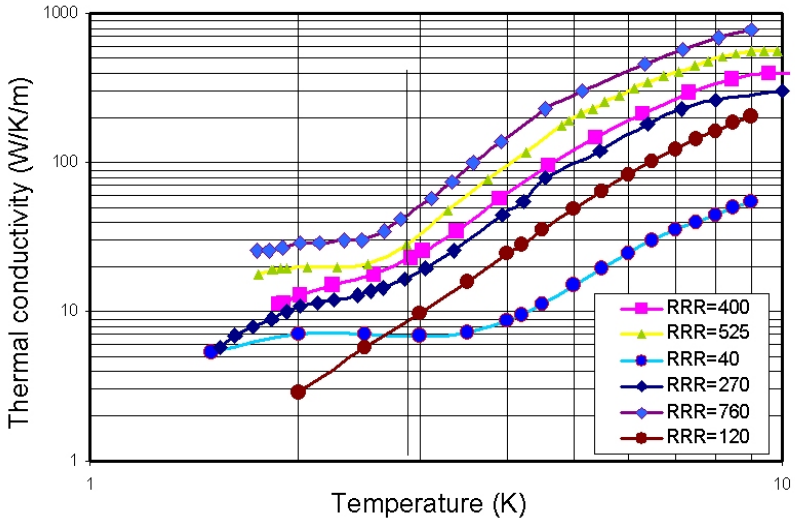

Figure 8: Thermal conductivity of Nb for SRF cavities. Courtesy of D. Reschke/DESY.

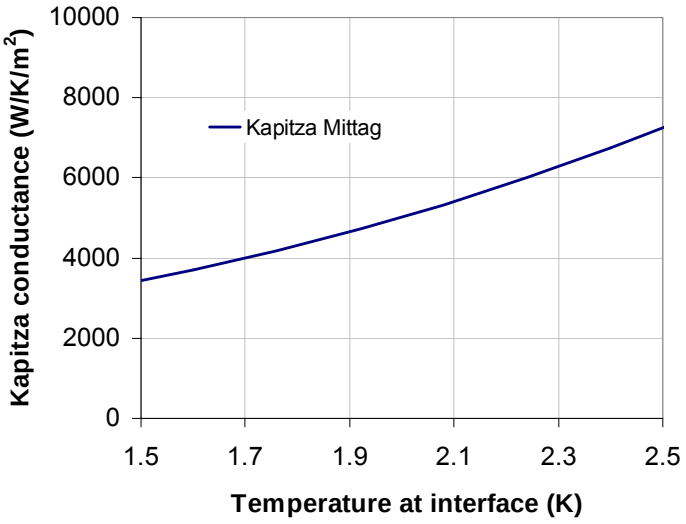

Figure 9: Kapitza conductance between Nb and HeII according to Mittag.

Appendix 2) Comparison of Different Implementations of Thermal Feedback

The following compares an analytical implementation of the thermal feedback model to the exact model (solutions of equations of 3&4). This comparison will reveal that the simplified model fails to describe the surface resistance when approaching the thermal quench condition. At fields below the quench field, however, the simplified model is a reasonable approximation of the thermal feedback process. The models described are –1- the so-called Haebel model, an analytical model which uses temperature independent properties and a first order Taylor expansion of the BCS surface resistance and –2- the exact model (i.e. the exact solution of Eqs. 3&4).

A2-1) Haebel's Analytical Model

A simplification, which is not necessarily accurate, but allows derivation of approximate solutions of the thermal feedback model, assumes that the thermal properties are assumed to be temperature independent. As discussed in section 2) this approximation is fairly accurate because the maximum temperature rise that can be tolerated on the surface before a thermal quench occurs because of the exponential temperature dependence of the BCS resistance. The material properties are typically calculated at the bath temperature T_0, the surface temperature T_m (on the RF exposed surface) or some average of them (referred to as T' here). With temperature independent thermal properties the heat balance equation (Eq. 1) becomes:

$$\boldsymbol{q_{heat} = P_{diss} = k_{therm}(T')(T_m - T_0)} \quad \left(\frac{\boldsymbol{W}}{\boldsymbol{m}^2}\right) \tag{A2-1}$$

The specific thermal conductance, k_{therm}, can be calculated from the thermal model representing the system. As shown in the schematic in Fig. 0 the thermal model is that of a series connection of the Nb thermal impedance and a Kapitza impedance at the Nb-He interface. This model assumes infinite conductance in the liquid helium, a good assumption in superfluid helium. In helium I this assumption is less good and an additional correction due to the thermal impedance of the helium itself would be needed.

$$k_{therm} = \frac{K_{therm}}{S} = \frac{1}{S}\frac{1}{R_{therm}} = \frac{1}{S}\frac{1}{\left(\frac{d}{\kappa_{Nb}S} + \frac{1}{h_{Kap}S}\right)} = \frac{\kappa h_{Kap}}{dh_{Kap} + \kappa} \quad \left(\frac{W}{K}\right) \tag{A2-2}$$

Equations (A2-1)-(A2-2) can be combined to an equation for the steady state temperature on the cavity surface T_m as a function of RF magnetic field amplitude. The thermal properties of the material are calculated at some particular temperature T'. In our case, in which $\kappa \sim h_{Kap}d$, the best choice is $T' \sim 0.5(T+T_0)$.

$$\boldsymbol{(T_m - T_0) = \frac{P_{diss}(T_m)}{k_{therm}(T')} = \frac{1}{2}\frac{dh_{Kap}(T') + \kappa(T')}{\kappa(T')h_{Kap}(T')} R_s(T_m) H_{RF}^2} \quad (\boldsymbol{K}) \tag{A2-3}$$

To solve Eq. (A2-3), an expression for the surface resistance $R_s(T)$ is needed. Typically a combination of residual and BCS surface resistance is used. Experimentally, the BCS resistance is derived from Q measurements in the cavity at different temperatures (and low power). The fit of the temperature dependence of the surface resistance allows to separate temperature dependent (BCS) and independent (residual,..) surface resistance contributions. This procedure is easiest at low field (low power). At high fields the disentanglement of the low and high field BCS contributions becomes more difficult.

Eq. (A2-3) can be solved easily with, for example, a solver in any commercial math software. An analytical thermal feedback model proposed in 1998 by E. Haebel, however, has been widely used to describe $Q(H_{RF})$ for SRF cavities. The Haebel model assumes that the BCS surface resistance can be expanded in a Taylor series as follows[5]

$$R_s(T) \approx R_s(T_0) + \left.\frac{\partial R_s}{\partial T}\right|_{T_0} \Delta T \tag{A2-4}$$

Here the temperature drop $\Delta T = T_m - T_0$ between the surface temperature T_m and bath temperature T_0 is assumed small, ($\Delta T << T_0$), so higher order terms in ΔT can be neglected. In turn, ΔT can be calculated from (A2-3), where all thermal parameters are taken at T_0. Substituting Eq. (A2-3) into Eq. (A2-4) and solving for $R_s(T)$, we obtain the non-isothermal surface resistance in the form:

$$\boldsymbol{R_s(H_{RF}) = \frac{R_s(T_0)}{1 - \left(\frac{dh_{Kap}(T_0) + \kappa(T_0)}{2\kappa(T_0) h_{Kap}(T_0)}\right) \left.\frac{\partial R_s(T)}{\partial T}\right|_{T_0} H_{RF}^2}} \tag{A2-5}$$

With Haebel we assumed $T'=T_0$ in Eq. (A2-5). For small RF field H_{RF}, Eq. (A2-5) simplifies to

$$\boldsymbol{R_s(H_{RF}) \approx R_s(T_0) \left[1 + \left(\frac{dh_{Kap}(T_0) + \kappa(T_0)}{2\kappa(T_0) h_{Kap}(T_0)}\right) \left.\frac{\partial R_s(T)}{\partial T}\right|_{T_0} H_{RF}^2\right]} \tag{A2-6}$$

Here dR_s/dT at T_0 can be calculated using the BCS surface resistance (6):

$$\boldsymbol{\left.\frac{\partial R_s}{\partial T}\right|_{T_0} = \left(R_s(T_0) - R_{s0}\right)\left(\frac{\alpha T_c}{T_0^2} - \frac{1}{T_0}\right)} \tag{A2-7}$$

Therefore, the Haebel model predicts a quadratic field dependence of $R_s(H_{RF})$ at small RF fields. It also predicts a thermal breakdown at the magnetic field H_b for which the denominator in Eq. (A2-5) goes to zero:

[5] "R&D Issues in Superconducting Cavities", presented at the TTF meeting 1998, DESY Internal Document TESLA-98-05 60, 1998;

$$H_b^2 = \frac{2\kappa(T_0)h_{Kap}(T_0)}{\left(dh_{Kap}(T_0)+\kappa(T_0)\right)\frac{\partial R_s(T)}{\partial T}\Big|_{T_0}} \qquad \text{(A2-8)}$$

As follows from Eq. (A2-5), the surface resistance $R_s(H_{RF})$ diverges at H_b indicating a main drawback of the Haebel model, which assumes that $T_m - T_0$ is small ($\Delta T << T_0$), so higher order terms in ΔT in Eq. (A2-4) are negligible. However, the fact that ΔT defined by Eqs. (A2-3) and (A2-5) becomes infinite at H_b, contradicts the initial assumption of the smallness of ΔT. This unphysical result indicates a mathematical inconsistency of the Haebel model, which gives incorrect behavior of $R_s(H_{RF})$ near the thermal breakdown field.

Appendix 3 describes a simple (and widely used) model that allows including other surface resistance contributions (e.g. non-linear BCS resistance terms) into the Haebel-model.

A2-2) Exact Model

The exact method consists of the simultaneous solution of Eqs. (3)&(4) using a numerical scheme. One possible solution consists of constructing two nested loops two temperature arrays that are systematically iterated through in small steps until T_s and T_m that solve Eqs. (3)&(4) for a given set of material properties and a chosen H_{RF} are found. The method used here in fact uses a built-in solver of a commercial math software to solve Eqs. (3)&(4). This method does not imply the calculation of the temperature profile across the Nb sheet (which is non relevant information anyways).

A2-3) Model Comparison

Table 3 gives "typical" material properties for a TESLA cavity. The BCS resistance parameters were derived from experimental data for one of the best performing 9-cell TESLA cavities (DESY AC70). The surface resistance implementation does not include the nonlinear correction. The thermal parameters in the table were calculated with the functions presented in Appendix 1. In particular the simplified fit (A1-6) was used to compute the Nb thermal conductivity (RRR=300, with phonon peak).

Different models were used to simulate the Q-slope of a TESLA cavity for the material parameters listed in Table 3. These are the analytical (Haebel) and numerical (exact) models. These models are discussed above. The quench at the critical field was not implemented in the models. The thermal quench field, calculated with the exact model is ~415 mT. Real cavities would obviously not be able to reach to the level of field because of the critical field limitation. This is of no importance here, however, since the purpose of the plots in Figure 10 and Figure 11 is to gauge semi- and analytical models by comparing them to the exact model.

Table 3: Material parameters used in the thermal model comparison.

parameter	symb	unit	value	comment
bath temperature	T_0	K	1.9	-
wall thickness	d	mm	2.6	
thermal conductivity at T_0	κ	W/m/K	11.2	w. phon peak, RRR=300
Kapitza conductance at T_0	h_{Kap}	$W/m^2/K$	5021	Mittag
BCS resistance parameter	$A(\omega)$	Ω	$1.058 \cdot 10^{-5}$	as in 1.3 GHz
BCS resistance parameter	α	-	1.94	DESY / A70 cavity
BCS resistance parameter	T_c	K	9.2	(after baking)
surface resistance at T_0	$R_s(T_0)$	Ω	$9 \cdot 10^{-9}$	includes 5 nΩ of R_{s0}

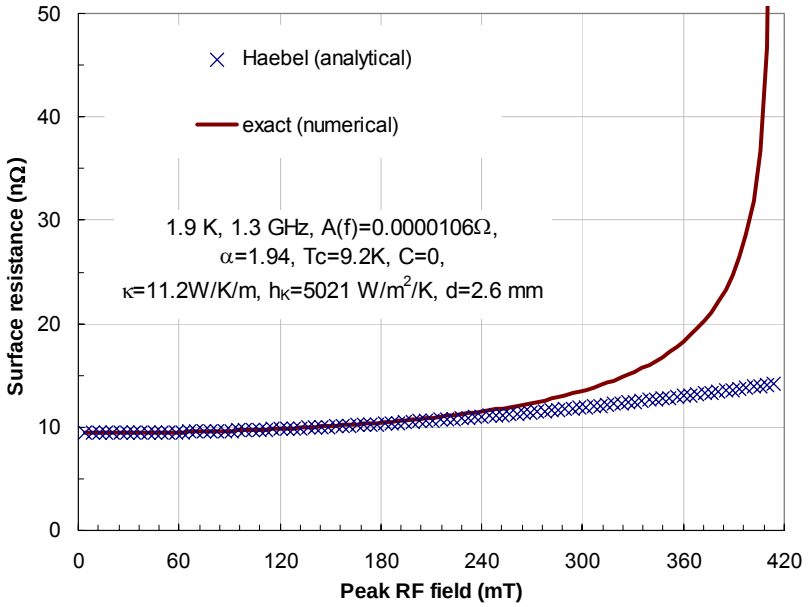

Figure 10: Comparison of surface resistance of a TESLA single cell cavity calculated with different implementations of the thermal feedback model and the material parameters as specified in Table 3.

The plots in Figure 10 and Figure 11 reveal that the analytical (Haebel) model is not well suited to predict the thermal breakdown. Especially the Haebel model also strongly under-estimates the Q slope at fields approaching the quench field. The medium field Q-slope due to thermal feedback, however, is reasonable well fitted with both implementations.

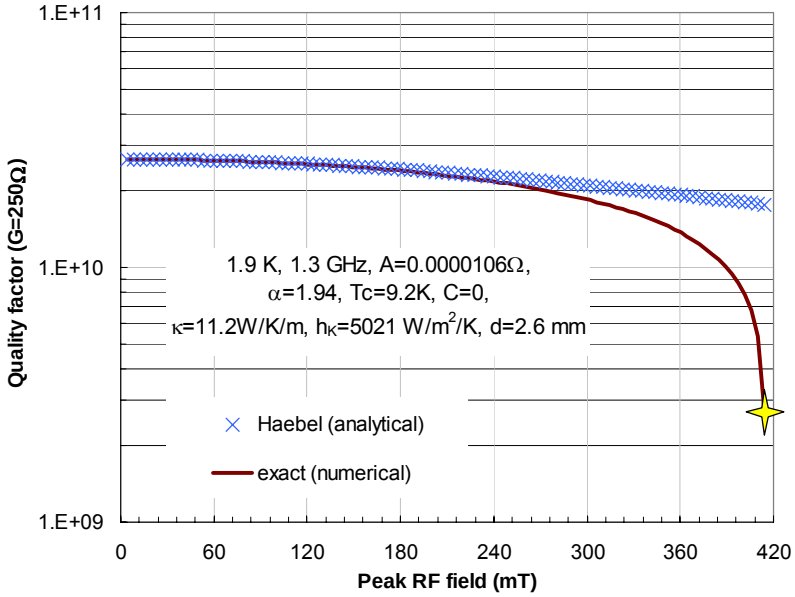

Figure 11: Comparison of quality factor of a TESLA single cell cavity calculated with different implementations of the thermal feedback model and the material parameters as specified in Table 3. The star indicates the thermal quench as predicted by the models.

Appendix 3) Calculation of γ

As suggested by J. Halbritter[6] the Haebel-model (see Appendix 2) can be generalized to include many different RF surface resistance contributions other than BCS. The starting point for this procedure is Eq. (A2-6) given in the derivation of the Haebel model in Appendix 2:

$$R_s(H_{RF}) \approx R_s(T_0)\left[1+\left(\frac{1}{2}\frac{dh_{Kap}(T_0)+\kappa(T_0)}{\kappa(T_0)h_{Kap}(T_0)}\right)\frac{\partial R_s(T)}{\partial T}\bigg|_{T_0} H_{RF}^2\right] \quad (\Omega) \qquad \text{(A3-1)}$$

To include, for example, the non-linear BCS contribution (according to Eq. 7), the linear BCS resistance term in Eq. (A3-1) needs to be multiplied with the field dependent non-linear correction term $(1+Ch^2)$, where h is the reduced field H_{RF}/H_c. This obviously assumes that $R_s=R_{res}+R_{s,bcs}$.

$$R_s(H_{RF}) \approx \left[R_{res}+R_{s,bcs}(T_0)\left[1+C\left(\frac{H_{RF}}{H_c}\right)^2\right]\right]\left[1+\left(\frac{1}{2}\frac{dh_{Kap}(T_0)+\kappa(T_0)}{\kappa(T_0)h_{Kap}(T_0)}\right)\frac{\partial R_s(T)}{\partial T}\bigg|_{T_0} H_{RF}^2\right] \quad (\Omega)$$

(A3-2)

Here C is assumed constant, so in terms of Eq. 8 $C=C(T_0,\omega)$. Retaining only the H terms with power smaller or equal than two one obtains:

$$R_s(H_{RF}) \approx R_s(T_0)\left[1+\left(\frac{C\left(\frac{R_{s,bcs}(T_0)}{R_s(T_0)}\right)}{H_c^2}+\frac{1}{2}\frac{dh_{Kap}(T_0)+\kappa(T_0)}{\kappa(T_0)h_{Kap}(T_0)}\frac{\partial R_s(T)}{\partial T}\bigg|_{T_0}\right)H_{RF}^2\right] = R_s(T_0)\left[1+\gamma\left(\frac{H_{RF}}{H_c}\right)^2\right] \quad (\Omega)$$

$$\gamma = \left(C\left(\frac{R_{s,bcs}(T_0)}{R_s(T_0)}\right)+\frac{1}{2}\frac{dh_{Kap}(T_0)+\kappa(T_0)}{\kappa(T_0)h_{Kap}(T_0)}\frac{\partial R_s(T)}{\partial T}\bigg|_{T_0} H_c^2\right) \qquad \text{(A3-3)}$$

As in (A2-6) dR_s/dT can be calculated at T_0 from Eq.6 (including the residual resistance R_{res}). A typical γ is of order unity (a calculation using the parameters in Table 3, gives γ ~2). As with the Haebel approximation, this model does not apply to the ultimate Q-drop close to the quench field.

[6] J. Halbritter, " Degradation of Superconducting RF Cavity Performances by Extrinsic Properties", Proc. of the XI[th] RF superconductivity workshop, Luebeck, Germany, 2003;